12th International Conference on Fracture Mechanics of Concrete and Concrete Structures
FraMCoS-12
B.L.A. Pichler, Ch. Hellmich, P. Preinstorfer (Eds)

https://doi.org/10.21012/FC12.1340
MS03-1:2

MONITORING OF CRACK PROPAGATION IN FIBER REINFORCED CONCRETES: COMPARISON OF NON-DESTRUCTIVE TECHNIQUES

T. BOUILLARD[*,†], A. TURATSINZE[*], J.P. BALAYSSAC[*], A. TOUMI[*], O. HELSON[†]

[*] Laboratoire Matériaux et Durabilité des Constructions de Toulouse (LMDC), Université de Toulouse INSA/UPS Génie-Civil, 135 Avenue de Rangueil, 31077 Toulouse, France.

[†] Agence nationale pour la gestion des déchets radioactifs (Andra), 1 rue Jean Monnet, 92290 Châtenay-Malabry, France.

e-mail: bouillar@insa-toulouse.fr

Key words: Structural Health Monitoring, Digital Image Correlation, Acoustic Emission, Optical Fibers, Electrical Measurement, Fiber-Reinforced Concrete.

Abstract: This study was carried out for the French National Radioactive Waste Management Agency (Andra) as part of the Cigéo project, a deep geological disposal facility for radioactive waste. Cigéo consists of a network of concrete galleries where the radioactive wastes will be disposed. After the construction and operation phase, the galleries will be sealed, and no further human intervention will be possible. Therefore, to monitor the health of the galleries remotely, structural health monitoring (SHM) techniques are required. The study focused on using three different monitoring techniques, namely acoustic emission (AE), strain measurements using optical fibers, and electrical measurements with embedded sensors to test the self-sensing ability of the concrete. The objective was to cross-reference data from these various techniques to propose methods for detecting cracks in concrete elements. The obtained results were compared with those from digital image correlation (DIC). These tests were carried out on structural elements, i.e. beams subjected to 4-point bending test. With the dual aim of improving the relevance of these monitoring techniques and better controlling crack propagation, fibers were incorporated into the concrete mixes. Two types of fibers were used: amorphous metallic fibers (AMF) and carbon fibers (CF). The results showed that CF primarily enhanced crack detection through electrical measurements without significant influence on mechanical performance. However, AMF demonstrated their ability to restrain crack propagation and improved the relevance of electrical and AE measurements to monitor crack initiation and propagation.

1. INTRODUCTION

This study, which was funded by Andra, focused on the detection of cracks in a reinforced concrete element containing fibers. Andra is currently working on the Cigéo project, a radioactive waste disposal facility. Located in France, this project aims to dispose high-level and intermediate-level long-lived radioactive waste for several thousand years.

Cigéo involves a network of underground tunnels located approximately 500 meters below the surface, within a stable clay layer known for being impermeable. The tunnels will be made of prefabricated reinforced concrete segments, with diameters reaching up to 12 meters. Given the challenges associated with the disposal of radioactive waste and the longevity of the structure, Andra attaches great importance to studying the durability of structures.

To reduce risks due to corrosion of the conventional steel rebars, Andra is studying alternative solutions using non-corrosive

fibers that could enhance mechanical performance, particularly in terms of crack control and strength. Specifically, the use of non-corrosive fibers in the concrete mix is being considered to reduce the amount of traditional reinforcement needed [1]-[2]-[3], and consequently decreasing corrosion risks.

In addition to durability challenges, structural monitoring is another concern. After an operational period during which waste will be placed in the tunnels, the project will be sealed and human access to the galleries will no longer be possible. As a result, various systems are being considered to ensure structural monitoring over time.

In this study, multiple monitoring systems were implemented to simultaneously track the initiation and propagation of cracks during bending tests on beams reinforced with both rebars and fibers. The different systems are:

- digital image correlation (DIC), that is a widely used technique to visually monitor the development of cracks [4].

- strain measurements using distributed optical fibers to detect cracks as soon as they are initiated [5].

- acoustic emission (AE) monitoring, that is based on the localization of acoustic events due to damage in concrete. This technique proved its relevance on many studies to monitor structural health [6]-[7].

- electrical measurements, that are also a way to monitor the damage based on the self-sensing capacity of concrete. Some researchers showed that electrical concrete resistance is impacted by the stress applied to it, as well as by the crack initiation and propagation [8].

The results from these various systems were cross-referenced to evaluate their accuracy and to propose structural monitoring methods to Andra.

2. MATERIALS AND METHODS

2.1. Materials

The concrete mixtures were composed of CEM III/A 52.5 L CE PM-ES-CP1 cement, calcareous filler, calcareous sand (0/4), and gravel (4/12). The dosage of super-plasticizer (SP) was adjusted to achieve a slump between 55 and 65 cm, ensuring the self-compacting properties of the concrete. Two types of fibers were used: amorphous metallic fibers (AMF) and carbon fibers (CF). Their dimensions are presented in Table 1. Amorphous metallic fibers, named F20L6 are provided by Saint-Gobain and the carbon fibers are provided by Toray Carbon and Apply Carbon. Both were selected for their durability and excellent corrosion resistance [9].

Table 1: Fibers dimensions

Fibers	l (mm)	w (mm)	t (mm)	d (µm)
AMF	30	1.6	0.029	-
CF	24	-	-	5-7

Where: l, is the length of the fiber, w, its width, t, its thickness, and d, its filament diameters.

Three different self-compacting concrete mixes were designed to obtain a C60/75 concrete. The plain concrete, named PC, was used as the reference sample. The mix named AMFRC was prepared with 30 kg/m^3 (0.41 % by volume) of AMF. Another mix, named CFRC, was prepared with 5 kg/m^3 (0.27 % by volume) of carbon fiber. All the details of the mixes are given in Table 2.

Table 2: Mix proportions

Component	AMFRC	CFRC	PC
Ciment (kg/m^3)	460	450	450
Filler (kg/m^3)	45	45	45
Sand (kg/m^3)	984	984	984
Gravel (kg/m^3)	659	672	672
Fiber (kg/m^3)	30	5	0
Water (kg/m^3)	187	187	187
SP (kg/m^3)	7.35	7.2	4.2
Slump (cm)	58	55	65

The volume fraction of CF was set at a lower level than that of the AMF because of the difficulties encountered in achieving sufficient slump, and because it was high enough to obtain good results in terms of self-sensing capability [10].

3. METHODS

3.1. Materials and experimental set-up

The beams tested in this study were 15 cm width, 28 cm height and 200 cm long. Longitudinal reinforcement consisted of 2Ø12 steel bar, and stirrups were Ø6.

Three beams (B1-AMF, B2-CF, B3-PC) were casted with the same steel reinforcement ratio, but with different concrete mixes:

- B1-AMF is made of mix AMFRC.
- B2-CF is made of mix CFRC.
- B3-PC is made of mix PC.

Four-point bending tests were conducted using a machine with a loading capacity of 200 kN. The experimental set-up is illustrated in Figure 1. The span length was set at 180 cm, and the distance between the two force application points was 50 cm.

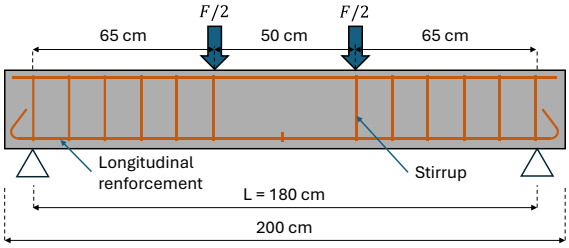

Figure 1: Test configuration.

The initial loading rate was selected so that the load increased at a constant rate of 8 kN/min until the first crack appeared. The first cracking load was pre-calculated and verified during the test. Once the beam cracked, the loading rate was controlled by the deflection at a rate of 10 mm/min until the end of the test. The measurement of the deflection was carried out using a LVDT sensor placed at mid-span of the beam.

3.2. Digital image correlation (DIC)

A digital image correlation system was installed to monitor the strain and crack opening on beam surface. To perform the measurements, a speckle pattern with 5 mm diameter dots was applied to one vertical face of the beam. Two high-resolution cameras were used to capture the data and Vic-Snap software was used for acquisition, while Vic3D processed the data. It allows the deformation field in the zone of interest to be calculated, and virtual displacement sensors can also be placed.

3.3. Acoustic emission (AE)

Acoustic emission measurement system consists of several components. Signals are captured by resonant piezoelectric sensors, fixed to the beam's surface with fast-setting silicone glue. The sensors are connected to 40 dB preamplifiers, then sent to a 8-channel acquisition board and processed using EAwin software. Eight sensors were placed on beam face (6 on the lateral face and 2 on the top face). The signal recording and filtering parameters were based on the work of A. Boniface [11]. The sensors were placed in a way that there is an average spacing of 30 cm between them. They were placed on the central part of the beam, between the two force application points, where most of the cracks are expected to occur.

3.4. Strain measurements with optical fiber

A distributed optical fiber was also installed in each beam to measure the strain of the concrete at the same height as the longitudinal reinforcements. This optical fiber, named FutureNeuro FN-SILL-3, is supplied by the company NEUBREX. Optical fiber was suspended from the longitudinal reinforcements using nylon threads, allowing the fiber to deform freely along the entire length of the beam. The fiber gives average strain values every 0.65 mm and the recording rate has been set to one measurement every 5 seconds.

3.5. Electrical measurements

Electrical measurements were recorded using a Wheatstone bridge with electrodes embedded in the concrete. The operating principle of the Wheatstone bridge is presented in the study of T. Ferdiansyah [12]. The electrodes, made of perforated metal plates measuring 6 × 10 cm, were placed 10 cm on either side of beam center, as illustrated on Figure 2. The electrodes were installed before casting, they were suspended from the rebar cage with nylon wire. A copper wire was threaded through the perforations in the plates to apply the electrical current. The copper wire extended to the top surface of the concrete, allowing connection to the rest of the Wheatstone bridge. A multimeter is connected to the bridge which records the change of the voltage that indicates a change in concrete electrical resistance.

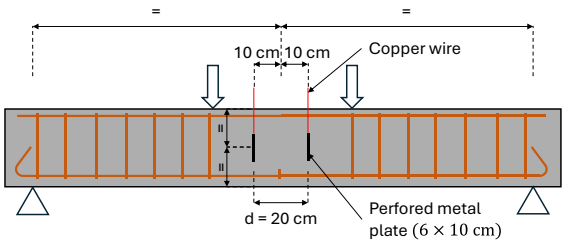

Figure 2: Electrodes set up.

4. RESULTS

4.1. Mechanical results

Figure 3 illustrates the mechanical behavior of the 3 beams subjected to four-point bending test. The three beams exhibit similar behavior, divided into three phases:

The first phase, referred to as the uncracked elastic phase, where the force-deflection curves are linear. During this phase, the concrete remains uncracked, and the stress level in the tensile zone is below the concrete's tensile strength. During this phase, neither the reinforcement bars nor the fibers are stressed. This phase ends when the force reaches the load initiating the first crack (denoted as F_{fc}), which corresponds to the force leading the tensile strength to be reached in the concrete's tensile zone.

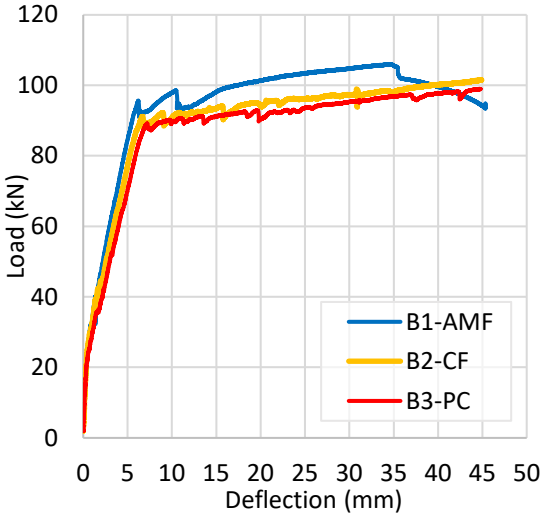

Figure 3: Load vs. deflection

The second phase, known as the cracked elastic phase, is still characterized by a linear relationship between force and deflection, but a change in slope compared to phase 1 is clearly noticeable. While the concrete is no longer in the elastic domain, the reinforcement bars still are. They continue to do so until yielding occurs, which is when the plasticity force (F_{plas}) is reached.

Then begins the third phase, which is not analyzed in this study, it is called the plasticity plateau. During this final phase, the force remains nearly constant until the beams fail.

Based on the behavior of these beams, comparative forces were established to serve as reference points for comparison of the behavior of the three beams. Those comparative forces are defined in Figure 4.

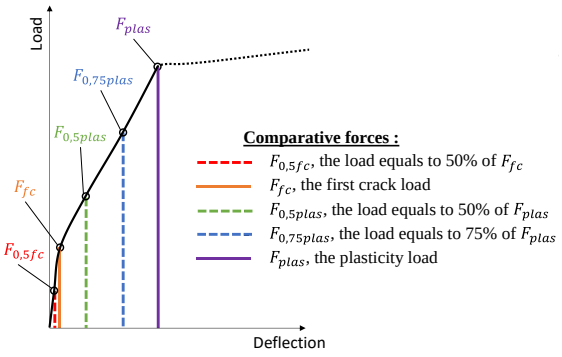

Figure 4: Definition of comparison forces.

The results given in Table 3 show that the three beams exhibit similar characteristic forces. However, beam B1, reinforced with AMF, seems to exhibit slightly higher values compared to the other two beams. These fibers have demonstrated their advantages at the material scale [13]-[14]-[15]-[16], and these tests have confirmed their effectiveness in hybrid reinforcement (fibers and rebars). Regarding carbon fibers, they did not result in significant improvements in terms of comparison forces.

Table 3: Comparative force values

Comparative forces	B1-AMF	B2-CF	B3-PC
$F_{0.5fc}$ (kN)	15.1	12.8	12.2
F_{fc} (kN)	30.1	25.5	24.4
$F_{0.5plas}$ (kN)	47.8	45.5	44.4
$F_{0.75plas}$ (kN)	71.7	68.3	66.6
F_{plas}(kN)	95.6	91.0	88.8

4.2. Crack development

To detect the initiation and propagation of cracks, virtual displacement sensors were used within DIC results. To do so, virtual sensors were positioned at the same height as the longitudinal reinforcement bars. They measure elongation at a given time and provide values at one-centimeter intervals along the beam's span.

Thus, when the beam is deformed, the sensors give a value of elongation and when a crack develops, a sudden elongation jump is observed. The magnitude of this jump corresponds to the crack opening.

To differentiate localized deformations from "true" cracks, a minimum jump threshold was calibrated at 0.04 mm. Below this value, the jump is disregarded; however, beyond this threshold, the jump indicates crack development. The value of this threshold is justified in the PhD thesis of T. Bouillard [10].

From the Figure 5 to Figure 7 are shown the crack positions and their opening values at various loading levels. For each loading level (from F_{fc} to F_{plas}), each detected crack is represented by a bar. The bar's height corresponds to the crack opening, and its position relative to the left support is plotted on the X-axis. In the case where a crack continues to grow at higher loading levels, the corresponding bar extends vertically while remaining at the same horizontal position.

For all beams, at the first cracking force (F_{fc}) one or two cracks, represented by orange squares in the figures, were detected in the central zone of the beams. These cracks all exhibited openings smaller than 0.05 mm.

By the loading level $F_{0.5plas}$, more cracks appeared, the cumulative crack opening detected by virtual displacement sensors, given in Figure 8, are 0.5 mm for B1, 0.84 mm for B2, and 1.13 mm. This means that, for equivalent loading levels, the AMFs reduced the cumulative crack opening by 48 % compared to beam B3-PC (without fibers). The CFs achieved a 25 % reduction. At the loading level $F_{0.75plas}$, the AMFs and CFs reduced the cumulative crack opening by 28 % and 10 %, respectively, compared to B3-PC.

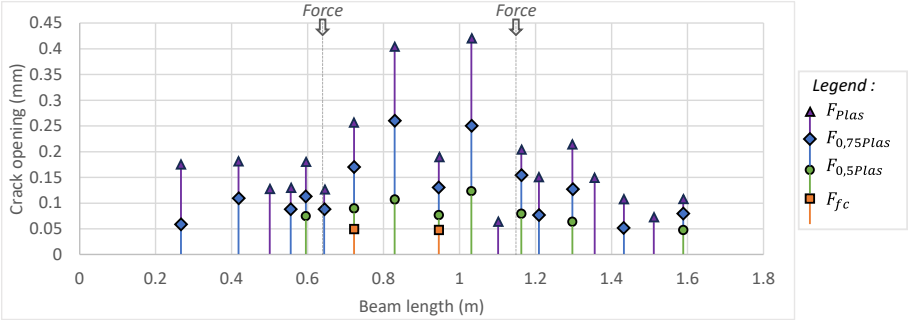

Figure 5: Crack development of B1-AMF.

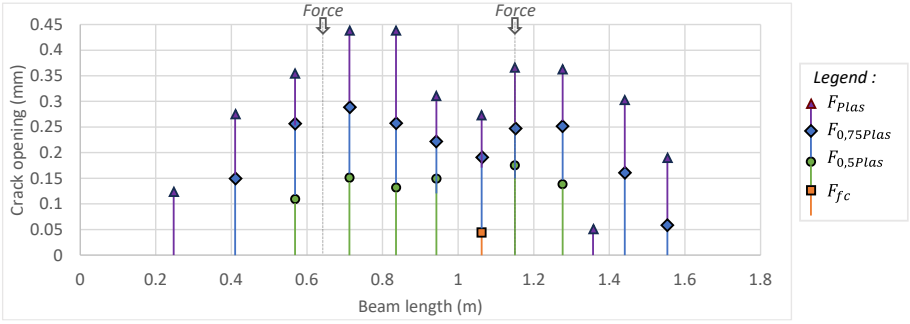

Figure 6: Crack development of B2-CF.

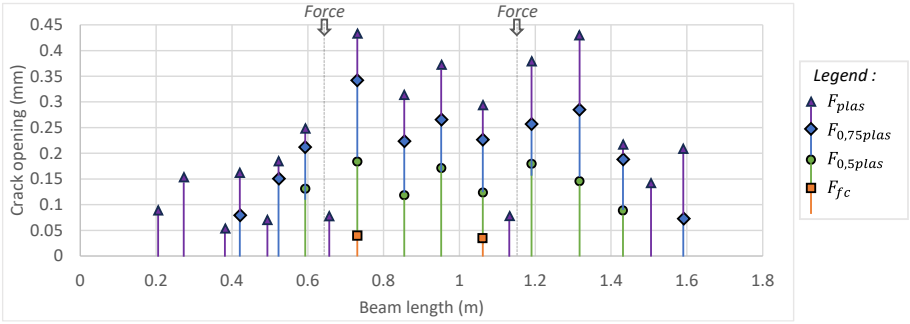

Figure 7: Crack development of B3-PC.

By comparing the cracking development of beams B2-CF and B3-PC, it can be noted that they are similar. Cracks developed evenly throughout the span. However, beam B1-AMF exhibits a different behavior. Two cracks, wider than the others, developed in the central part of the beam. These cracks coincide with the position of the metal plates used as electrodes for electrical measurements. The proposed hypothesis is that these electrodes caused preferential cracking at this location. Indeed, these plates locally created an area where the fibers could not perform their bridging function. Finally, at the F_{plas}, the reductions of cumulative crack opening were 19 % and 10 % for the AMFs and CFs, respectively. Despite this result, CF does not seem to play a major role in limiting cracking. Indeed, even though the cumulative crack opening at F_{plas} is slightly lower than for B3-PC, the force at which it was calculated is also slightly lower (approximately 2.5 %). In contrast, for beam B1-AMF, the cumulative crack opening is reduced by 19%, while F_{plas} is 5% higher.

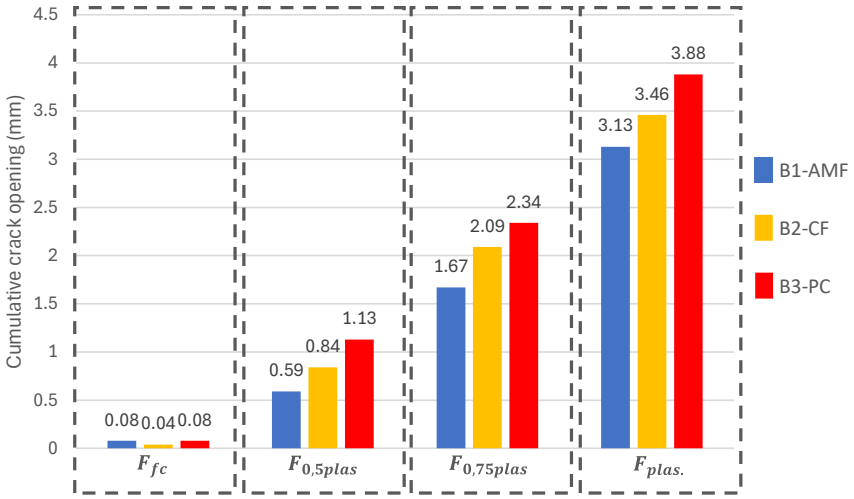

Figure 8: Cumulative crack opening at F_{fc}, $F_{0.5pas}$, $F_{0.75plas}$ and F_{plas}.

4.3. Strain measurements with distributed optical fibers

The results obtained by the distributed optical fibers are given from Figure 9 to Figure 11. For each beam, strains are recorded at loading levels ranging from the preload phase to approximately 20 kN. Beyond this value, the optical fibers seem to be debonded from the matrix, distorting the measurements.

Results show localized strains that are the precursors of the first cracks. In fact, while the applied force is only about two-thirds of F_{fc}, highly localized peaks of strain are already observed although beams are not considered as cracked.

By cross-referencing these results with those from the DIC (illustrated by black dashed lines), it can be concluded that all cracks detected by the DIC correspond to peaks in strain field measured by the optical fibers. However, the reverse is not true. The optical fibers detect highly localized deformations that do not appear in the DIC data. This discrepancy arises because the optical fibers can measure deformations at very low loading levels, whereas the DIC lacks such accuracy.

Moreover, it is possible that cracks do not develop uniformly within the concrete volume. Cracks may initially form internally and only become visible on the surface after a certain period or loading threshold.

The optical fiber thus appears to be an effective way of detecting strain localization and imminent initiation of cracks. Indeed, theoretical calculations and DIC have shown that cracks form around 25 to 30 kN for all beams (see paragraph 4.2). However, with optical fiber measurements, it is possible to clearly identify the appearance of highly localized strains as early as the application of a force of 15 to 20 kN.

The results of B1-AMF show that, unlike the others, this beam exhibits multiple localized strain before reaching F_{fc}. Indeed, at a force of 22 kN, there are four strain peaks exceeding 100 µm/m. In contrast, for the other two beams, only one peak was observed at equivalent load levels. It is possible that the AMF generate more distributed strain along the length, which could be the first signs of multi-cracking at higher load levels.

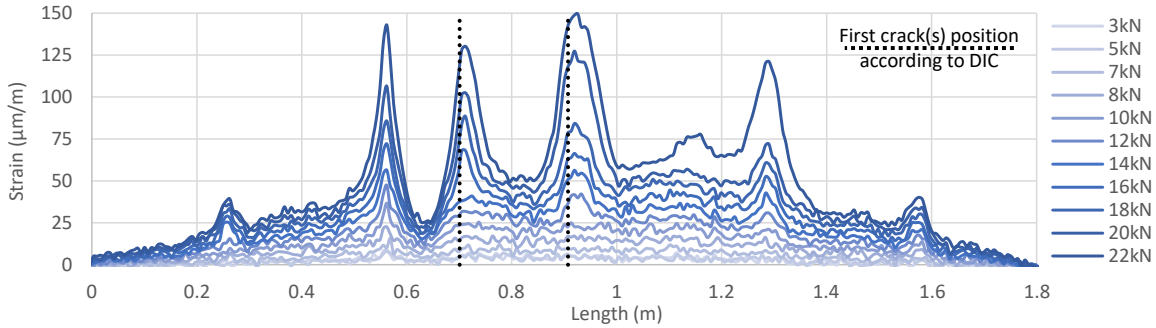

Figure 9: Strain measurements of B1-AFM.

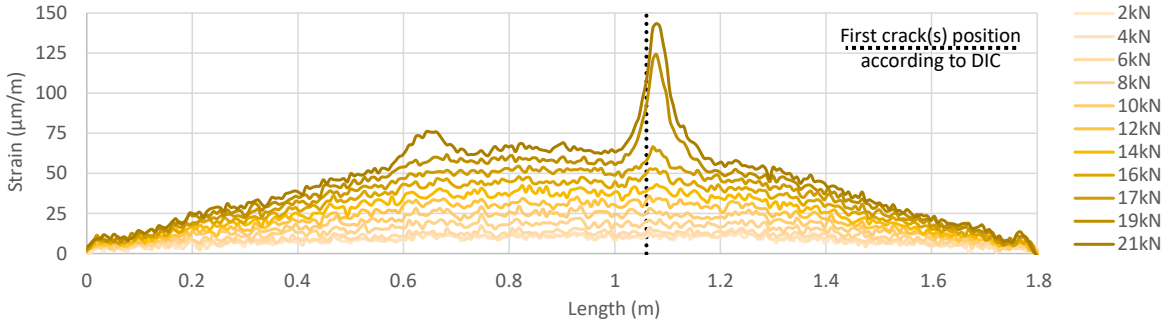

Figure 10: Strain measurements of B2-CF.

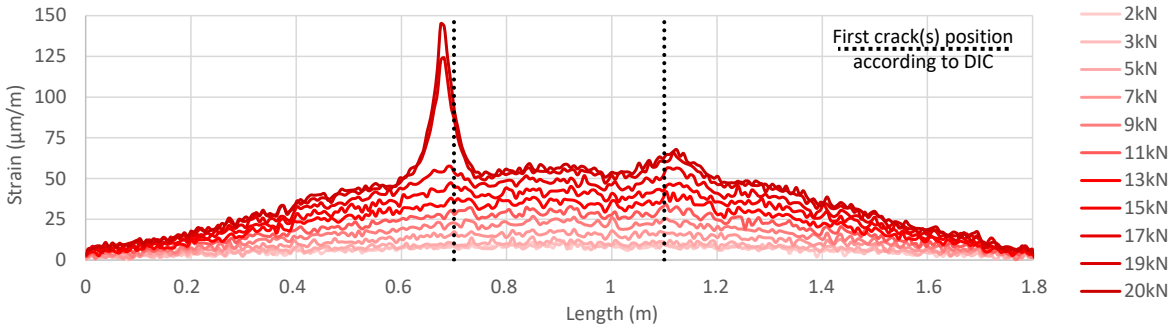

Figure 11: Strain measurements of B3-PC.

4.4. Crack detection using AE

The localization of acoustic events (EA) was performed using the AEWin software with a simplex resolution method. Each acoustic event is defined by its position along the span (x), the height of the beam (y), and the time at which the event occurred. By analyzing the distribution of events along the length of the beams, it is possible to identify areas where acoustic events were most frequent. The localization of damage can be done along the beam's length by counting the number of events detected at a given x value, each section was set to 1 cm.

The results from Figure 12 to Figure 14 show the distribution of acoustic events along the length of the beams from the beginning of the test until the force F_{fc} is reached. These results have been combined in the same graphs with the positions of the first cracks detected by DIC.

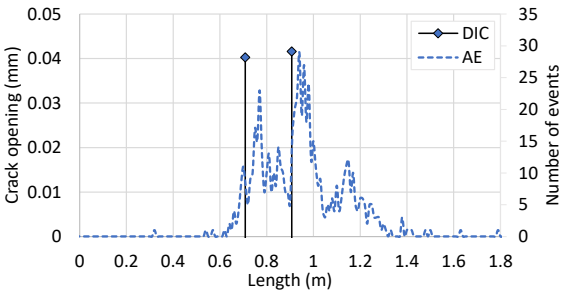

Figure 12: Crack localization with EA vs DIC – B1-AFM.

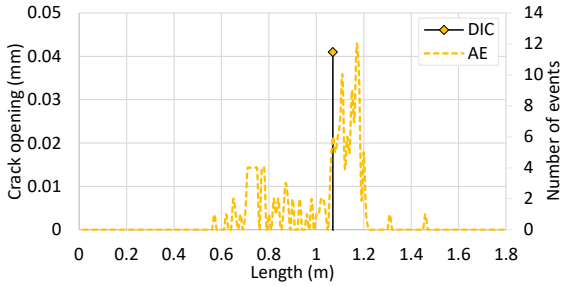

Figure 13: Crack localization with EA vs DIC – B2-CF.

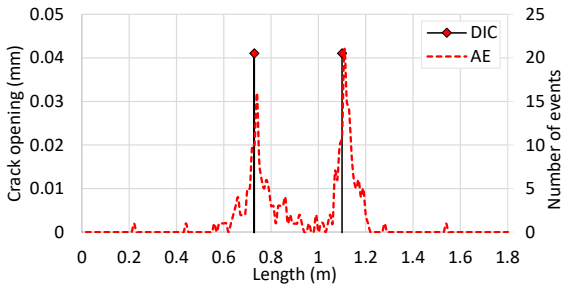

Figure 14: Crack localization with EA vs DIC – B3-PC.

In all three cases, a peak in acoustic events was observed at the same position as the cracks measured by DIC. A slight shift was noted for beams B1 and B2, which can be explained by the difference in observation methods. DIC captures only the surface, while acoustic measurements span the entire section. Thus, if the crack doesn't develop orthogonally to the DIC-observed face, the locations may differ. However, for beam B3-PC, the results show a strong correlation between the two measurement techniques. It is worth noting that for equivalent crack openings (around 0.04 mm), the number of acoustic events varies depending on the beam. At the force F_{fc}, 631 acoustic events were detected for B1-AMF, 162 for B2-CF, and 261 for B3-PC. Acoustic events are emitted when beams are damaged. The higher number of events in beam B1 suggests that the amorphous metal fibers generate acoustic signals when they are stressed or broken. Carbon fibers, due to their small dimensions (7 µm diameter, as a reminder) may not generate acoustic events when their failure occur. Further studies are planned to differentiate acoustic events originating from the matrix, fiber sliding or fiber breaking depending on signal parameters received.

4.5. Crack detection using electrical measurement

For processing results obtained from electrical measurements using the Wheatstone bridge, the results were cross-referenced with DIC. To achieve this, a virtual strain gauge was placed between the two points of force application (a 50 cm sensor located at mid-span of the beam, 3 cm from the underside). The results are presented in Figure 15, which shows the evolution of the voltage within the Wheatstone bridge as a function of the virtual strain gauge's elongation. As a reminder, the change of the voltage (ΔV) indicates a change in concrete resistance.

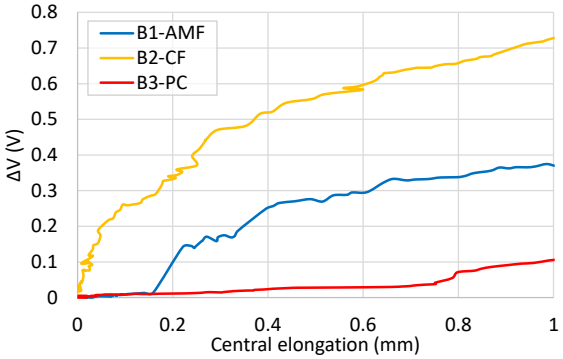

Figure 15: ΔV vs the central elongation.

The results show three different responses. Beam B3-PC exhibits a delayed response and low sensitivity, resulting in a limited evolution of ΔV even at advanced elongation levels. Without fibers, the changes in electrical properties are exclusively induced by modifications in the microstructure. This corresponds to electrolytic conductivity where the electrical current flows through the more or less saturated porous solution [17]. When a tensile force is applied, the pores deform, and cracks may initiate within the concrete volume, thereby altering the connectivity of the pores. Consequently, the electrical resistivity of the concrete increases [18]. The opposite phenomena are observed in the case of compression [19]-[20].

To understand why B3-PC response is delayed, it is important to note that during bending, the lower part of the beam is subjected to tension, while the upper part is subjected to compression stress. These two types of stress tend to produce opposite effects on the electrical resistivity of the concrete.

Thus, at the start of the test, when the neutral axis of the beam is almost at mid-height, the effect of the compressed part is counterbalanced by that of the tensioned part. However, as the load level increases, the neutral axis rises progressively, and the tensioned part becomes dominant over the compressed part until the concrete cracks. From that point onward, the impact of the compressed part becomes lower compared to that of the tensioned part.

In the case of beam B2-CF, the carbon fibers, due to their conductivity, make the concrete more sensitive, meaning that for the same elongation value, the corresponding ΔV is much higher than for the other beams. Moreover, the electrical measurements evolve simultaneously with the beam's deformation, since the start of the loading. With carbon fibers, the conductivity of the concrete is significantly increased [21].The electrical conductivity becomes both electrolytic and electronic. The current can also flow through the fibers. Thus, when the concrete cracks and/or deforms, the connections between the fibers are altered. As the material deforms, the distances between the fibers change, affecting the ability of electrons to move from one fiber to another. Fibers located at the cracks may also break, lowering the electronic conductivity.

For beam B1-AFM, there is an initial phase during which the electrical response is very low. It is only from approximately 0.15 mm of elongation that the electrical response becomes significant. For this beam, the same physical phenomena as the for B2-CF drive the evolution of electrical resistivity.

The question now arises as to why the fibers provide better sensitivity and an earlier response. The assumed hypothesis is based on the principle of percolation. Assuming that percolation is achieved, the fact that the fibers come closer together in the compressed region has no significant effect on resistivity. However, in the tensioned region, the fibers move apart and may break, which increases resistivity. Thus, carbon fibers could bypass the decrease in resistivity in the compressed region and focus on the effects of the tensioned region. With amorphous metallic fibers, since percolation is probably not achieved, this phenomenon may still occur but with less accuracy.

The addition of fibers therefore enhances the effectiveness of this technique for crack monitoring by improving sensitivity and, more importantly, enabling a significant response even at very low elongation levels.

5. CONCLUSION

This study highlighted monitoring techniques for crack detection at the scale of structural elements. The four techniques presented each have their own advantages and limitations.

DIC provides extensive information about the cracking levels in beams. It allowed the detection of crack initiation and the monitoring of their propagation during the tests. However, it is challenging to implement and requires significant post-processing work. Furthermore, the analysis is carried out only on the surface of the beam, which may not fully represent the entire volume of the concrete.

Distributed optical fibers were able to detect the early onset of cracks with high accuracy. However, this technique poses significant challenges in monitoring strain near cracks and estimating quantitively crack openings [22]. These difficulties are even more pronounced in elements exhibiting multiple cracking [23].

Acoustic emission appears to be an effective method for detecting crack initiation. It enabled the determination of the position of acoustic events that coincided with the location of cracks. Moreover, the measurements cover the entire concrete volume, making the data more representative. However, the analysis performed does not differentiate between events caused by fibers sliding or breaking and those caused by the cement matrix cracking, though more advanced analysis is planned.

Finally, electrical measurements demonstrated that with the addition of fibers, this technique becomes a promising one. For structural applications, it could serve as an alert system when a certain level of voltage variation is observed. Similar to acoustic emission, this technique also provides information about the concrete volume as a whole. However, to be effective, the electrodes must be placed in critical areas where cracks are most likely to form. Additionally, the inclusion of fibers seems essential, as without them, the concrete exhibits low sensitivity. Moreover, without fibers, the resistivity of the concrete becomes very sensitive to variations in its saturation level [24] which could lead to misinterpretations.

6. REFERENCES

[1] Y. Fritih, "Apport d'un renfort de fibres sur le comportement d'éléments en béton autoplaçant armé," Université de Toulouse, INSA, 2009.

[2] J. M. Yang, J. K. Kim, and D. Y. Yoo, "Flexural and shear behaviour of high-strength SFRC beams without stirrups," *Mag. Concr. Res.*, vol. 71, no. 10, pp. 503–518, 2018, doi: 10.1680/jmacr.17.00462.

[3] R. Narayanan and I. Y. S. Darwish, "Use of Steel Fibers As Shear Reinforcement," *ACI Struct. J.*, vol. 84, no. 3, pp. 216–227, 1987, doi: 10.14359/2654.

[4] D. C. T. Cardoso, G. B. S. Pereira, F. A. Silva, J. J. H. Silva Filho, and E. V. Pereira, "Influence of steel fibers on the flexural behavior of RC beams with low reinforcing ratios: Analytical and experimental investigation," *Compos. Struct.*, vol. 222, p. 110926, 2019, doi: 10.1016/j.compstruct.2019.110926.

[5] O. Fischer, S. Thoma, and S. Crepaz, "Distributed fiber optic sensing for crack detection in concrete structures," *Civ. Eng. Des.*, vol. 1, no. 3–4, pp. 97–105, 2019, doi: 10.1002/cend.201900008.

[6] B. Schechinger and T. Vogel, "Acoustic emission for monitoring a reinforced concrete beam subject to four-point-bending," *Constr. Build. Mater.*, vol. 21, no. 3, pp. 483–490, 2007, doi: 10.1016/j.conbuildmat.2006.04.003.

[7] A. C. Mpalaskas, T. E. Matikas, D. G. Aggelis, and N. Alver, "Acoustic emission for evaluating the reinforcement effectiveness in steel fiber reinforced concrete," *Appl. Sci.*, vol. 11, no. 9, 2021, doi: 10.3390/app11093850.

[8] J. Han *et al.*, "Development of self-sensing engineered cementitious composite sensors for monitoring flexural performance of reinforced concrete beam," *Dev. Built Environ.*, vol. 18, no. March, 2024, doi: 10.1016/j.dibe.2024.100407.

[9] J. Catalot, "Résistance à la corrosion des fibres métalliques amorphes Application à la réparation des collecteurs par béton projeté fibré," *7ème Congrès Int. CEOCOR*, 2006.

[10] T. Bouillard, "Optimisation et caractérisation d'un béton haute performance renforcé par des fibres résistantes à la corrosion," p. 285, 2024.

[11] A. Boniface, "Détection et évaluation de l'endommagement mécanique du béton par émission acoustique," Université de Bordeaux, 2018.

[12] T. Ferdiansyah, J. P. Balayssac, and A. Turatsinze, "An Experimental Approach for Characterisation of Concrete Damage Using the Wheatstone Bridge Circuit," *Int. J. Civ. Eng.*, vol. 0123456789, 2021, doi: 10.1007/s40999-021-00659-z.

[13] R. Hameed, A. Turatsinze, F. Duprat, and A. Sellier, "Metallic fiber reinforced concrete: Effect of fiber aspect ratio on the flexural properties," *J. Eng. Appl. Sci.*, vol. 4, no. 5, pp. 67–72, 2009.

[14] T. Bouillard, A. Turatsinze, O. Helson, J. Balayssac, A. Toumi, and C. Soula, "Mechanical performance and self-sensing capability of an amorphous fiber-reinforced concrete for radioactive waste storage facilities," vol. 431, no. September 2024, 2025, doi: 10.1016/j.nucengdes.2024.113727.

[15] H. Kim, G. Kim, J. Nam, J. Kim, S. Han, and S. Lee, "Static mechanical properties and impact resistance of amorphous metallic fiber-reinforced concrete," *Compos. Struct.*, vol. 134, pp. 831–844, 2015, doi: 10.1016/j.compstruct.2015.08.128.

[16] K. K. Choi and D. O. Ku, "Flexural behaviour of amorphous metal-fibre-reinforced concrete," *Proc. Inst. Civ. Eng. Struct. Build.*, vol. 168, no. SB1, pp. 15–25, 2014, doi: 10.1680/stbu.13.00045.

[17] H. W. Whittington, J. McCarter, and M. C. Forde, "The conduction of electricity through concrete," *Mag. Concr. Res.*, vol. 33, no. 114, pp. 48–60, 1981, doi: 10.1680/macr.1981.33.114.48.

[18] A. Peled, J. M. Torrents, T. O. Mason, S. P. Shah, and E. J. Garboczi, "Electrical impedance spectra to monitor damage during tensile loading of cement composites," *ACI Mater. J.*, vol. 98, no. 4, pp. 313–322, 2001, doi: 10.14359/10400.

[19] P.-W. Chen and D. D. L. Chung, "Concrete as a new strain/stress sensor," *Composites*, pp. 11–23, 1995.

[20] S. Ding, S. Dong, A. Ashour, and B. Han, "Development of sensing concrete: Principles, properties and its applications," *J. Appl. Phys.*, vol. 126, no. 24, 2019, doi: 10.1063/1.5128242.

[21] M. Chiarello and R. Zinno, "Electrical conductivity of self-monitoring CFRC," *Cem. Concr. Compos.*, vol. 27, no. 4, pp. 463–469, 2005, doi: 10.1016/j.cemconcomp.2004.09.001.

[22] H. Zhang and Z. Wu, "Performance Evaluation of PPP-BOTDA-Based Distributed Optical Fiber Sensors," vol. 2012, 2012, doi: 10.1155/2012/414692.

[23] A. Bassil, X. Chapeleau, D. Leduc, and O. Abraham, "Concrete Crack Monitoring Using a Novel Strain Transfer Model for Distributed Fiber Optics Sensors," pp. 1–17, 2020, doi: 10.3390/s20082220.

[24] J. K. Su, C. C. Yang, W. B. Wu, and R. Huang, "Effect of moisture content on concrete resistivity measurement," *J. Chinese Inst. Eng.*, vol. 25, no. 1, pp. 117–122, 2002, doi: 10.1080/02533839.2002.9670686.